Discretization Methods for Quantum Drift-Diffusion Model: A Comparison Based on the Quasi-Fermi Scheme

Pengcong Mu[1,2], Tao Cui[2,3], Lang Zeng[4], Xiaoyue Feng[1,2], Kun Luo[1,2], Zhiqiang Li[1,2*]
[1] Institute of Microelectronics, Chinese Academy of Sciences, Beijing 100029, China.
[2] University of Chinese Academy of Sciences, Beijing 100049, China.
[3] LSEC, NCMIS, Institute of Computational Mathematics and Scientific Computing, Academy of Mathematics and Systems Science, Chinese Academy of Sciences, Beijing 100190, China.
[4] School of Integrated Circuit Science and Engineering, Beihang University, Beijing 100191, China.
*Email: lizhiqiang@ime.ac.cn

***Abstract*—This paper investigates four discretization schemes–EAFE, FVSG, CVFEM-SG, and EFTFE–for solving the quantum drift-diffusion (QDD) model formulated using quasi-Fermi levels. A series of simulations on a 10 nm gate-all-around (GAA) transistor are conducted across various mesh types, including structured and non-Delaunay grids. The methods are evaluated in terms of accuracy, numerical stability, and computational efficiency. Among them, the EAFE method consistently demonstrates high accuracy and robust convergence behavior, exhibiting strong mesh-independence and superior overall performance.**

***Index Terms*—Quantum drift-diffusion model, Quasi-Fermi scheme, Discretization methods, Finite element method, Finite volume method, GAAFET**

I. Introduction

The continued downscaling of semiconductor devices has significantly amplified the influence of process-induced morphological variations on device performance. Meshes generated through process emulation are typically non-Delaunay [1], which presents significant challenges to the stability and accuracy of Voronoi-based finite volume device simulators. Over the years, numerous discretization schemes have been proposed, many originating from the classical Scharfetter–Gummel (SG) method. However, their effectiveness in addressing the challenges posed by modern device geometries and quantum-scale effects remains an open question.

Among quantum-corrected transport models, the quantum drift-diffusion (QDD) model, also known as the density-gradient model, remains one of the most computationally efficient approaches for capturing quantum confinement effects. It continues to see widespread use in both academic research and industrial simulation workflows. While various discretization methods for the conventional drift-diffusion (DD) model have been studied extensively [2], [3], the QDD model introduces fundamentally different mathematical properties. To date, systematic comparisons of discretization schemes specifically tailored for the QDD model remain scarce in the literature.

In this work, we examine four representative discretization approaches: the edge-averaged finite element (EAFE) method [4], the finite volume Scharfetter–Gummel (FVSG) method, the control volume finite element method with multidimensional Scharfetter–Gummel upwinding (CVFEM-SG) [5], and the exponentially fitted tetrahedral finite element (EFTFE) method [6]. These methods are applied to the QDD model formulated using quasi-Fermi levels, a formulation that has shown particular advantages in simulating cryogenic, wide-bandgap, and high-voltage devices [7]. We compare the methods in terms of accuracy, numerical stability, and computational efficiency through simulations of a gate-all-around (GAA) device using various mesh configurations.

II. Methods

A. Physical Model

The QDD model, utilizing the exponential transformation of carrier density variables $n/n_i = e^{2\psi_n}$ and $p/n_i = e^{2\psi_p}$, can be formulated as follows [8]:

$$-\nabla\cdot(\epsilon\nabla\phi) = q(n_i e^{2\psi_p} - n_i e^{2\psi_n} + D), \tag{1}$$

$$\nabla\cdot\boldsymbol{J}_n = R, \quad \boldsymbol{J}_n = -\mu_n n_i e^{2\psi_n}\nabla\phi_n, \tag{2}$$

$$\nabla\cdot\boldsymbol{J}_p = -R, \quad \boldsymbol{J}_p = -\mu_p n_i e^{2\psi_p}\nabla\phi_p \tag{3}$$

$$\nabla\cdot(2b_n\nabla e^{\psi_n}) = e^{\psi_n}(\phi_n - \phi + 2V_{th}\psi_n), \tag{4}$$

$$-\nabla\cdot(2b_p\nabla e^{\psi_p}) = e^{\psi_p}(\phi_p - \phi - 2V_{th}\psi_p), \tag{5}$$

where ϕ is the electrostatic potential, ϕ_n, ϕ_p are the electron and hole quasi-Fermi potentials, $\boldsymbol{J}_n$, $\boldsymbol{J}_p$ are the current densities for electrons and holes, q is the electronic charge, ϵ is the dielectric constant of the material, D and R denote the doping profile and net recombination rate, and $b_n = \frac{\gamma_n\hbar^2}{12qm_n^*}$, $b_p = \frac{\gamma_p\hbar^2}{12qm_p^*}$ are the density-gradient coefficients.

B. Discretization Schemes

Equations (1) and (4) - (5) are discretized using the standard Galerkin finite element method (FEM) and the interpolated-exponential finite element (IEFE) scheme, as detailed in [8]. For the carrier continuity equations (2) - (3), we refer the reader to [8] for the complete formulation of the EAFE method. Different from the FVSG method, which approximates the current density flux $\boldsymbol{J}_n\cdot\boldsymbol{n}$ along mesh edges as a constant, the EAFE method approximates the vector field $\boldsymbol{J}_n$ as a constant within each tetrahedral element.

The CVFEM-SG approach [5] approximates $\boldsymbol{J}_{n/p}$ in the lowest-order Nédélec edge element space $\boldsymbol{P}^{\mathcal{N}}(\Omega)$ via an edge

element lifting of the 1D SG edge currents. For electrons, the current density is given by

$$\boldsymbol{J}_n \approx \sum_{E\in E(\Omega)} |E| J_{ij} \vec{\boldsymbol{W}}_{ij},$$

where $\vec{\boldsymbol{W}}_{ij}$ is the basis of $\boldsymbol{P}^{\mathcal{N}}(\Omega)$ on edge $E : \boldsymbol{A}_i^E \to \boldsymbol{A}_j^E$ and J_{ij} is the SG edge current densities

$$J_{ij} = -\mu_n/|E| \left[e^{2\psi_{n_i}} B(\Delta)\phi_{n_i} - e^{2\psi_{n_j}} B(-\Delta)\phi_{n_j} \right],$$
$$\Delta = 2\psi_{n_i} - 2\psi_{n_j}, \quad B(x) = x/(e^x - 1).$$

For the EFTFE method [6], the weak formulation of (2) is written as:

$$-(\boldsymbol{J}_n, \nabla v) = (\sqrt{\mu_n} e^{\psi_n} \nabla \phi_n, \sqrt{\mu_n} e^{\psi_n} \nabla v) = (R, v).$$

This leads to a system using exponential basis functions defined over each tetrahedron. For the basis function $b_1(x)$ and auxiliary flux $\boldsymbol{p}_1(x)$ associated with vertex $\boldsymbol{A}_1$, the relation

$$\frac{\boldsymbol{p}_1(x) \cdot \boldsymbol{l}_m}{\sqrt{\mu_n}} = B(\sigma_m) e^{\psi_n(x)} b_1(x) - B(-\sigma_m) e^{\psi_n(\boldsymbol{A}_m)} \delta_{1m},$$

holds for $m = 1, 2, 3, 4$, where $\boldsymbol{l}_m := x - \boldsymbol{A}_m$, $\sigma_m := \nabla\psi_n \cdot \boldsymbol{l}_m$, and δ_{1m} is the Kronecker delta.

C. Nonlinear Solvers and Linear System Solution

To handle the nonlinear coupling in the QDD equations, a monolithic Newton solver is employed for the EAFE, FVSG, and CVFEM-SG discretizations. For EFTFE, the Gummel iteration is used due to the complexity of forming the Jacobian. At each nonlinear step, the resulting linear system is solved using either a parallel direct sparse solver (MUMPS) or an algebraic multigrid (AMG)-preconditioned flexible GMRES (FGMRES) method.

III. Results

To evaluate the performance of the EAFE, FVSG, CVFEM-SG, and EFTFE discretization schemes applied to the QDD model, we consider a benchmark simulation of an n-type GAAFET with a gate length of 10 nm. The source and drain regions are defined by two 5×5 nm contacts, as illustrated in Fig. 1. The accuracy of the simulation framework has been validated in previous work [8]. Four finite element meshes are employed for comparison (see Fig. 1):

- (a) **mesh Good:** all tetrahedral elements have dihedral angles $\leq \pi/2$;
- (b) **mesh S:** generated using a commercial mesh generator;
- (c) **mesh Unstructured:** an unstructured tetrahedral mesh generated by TetGen [9];
- (d) **mesh Non-Delaunay:** obtained by applying three successive longest-edge bisections starting from a structured mesh configuration similar to that in Fig. 1(b).

For reference, Fig. 2(a) and 2(b) show the tetrahedral subdivisions of a unit cube corresponding to mesh Good and mesh S, respectively.

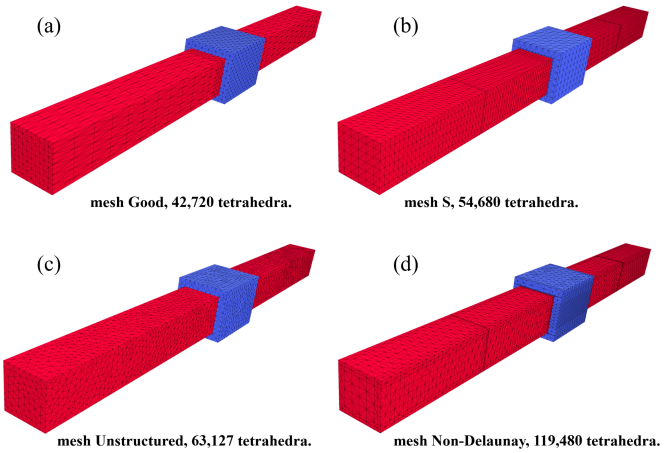

Fig. 1. Device structure and four types of tetrahedral meshes used in the GAAFET simulation.

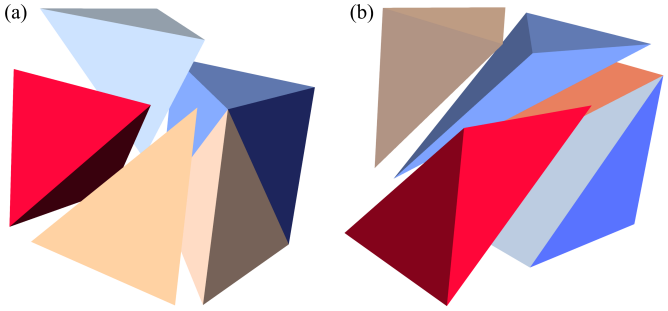

Fig. 2. Tetrahedral subdivision of a unit cube corresponding to: (a) the mesh with dihedral angle $\leq \pi/2$ (as in Fig. 1(a)). (b) the mesh generated by a commercial tool (as in Fig. 1(b)).

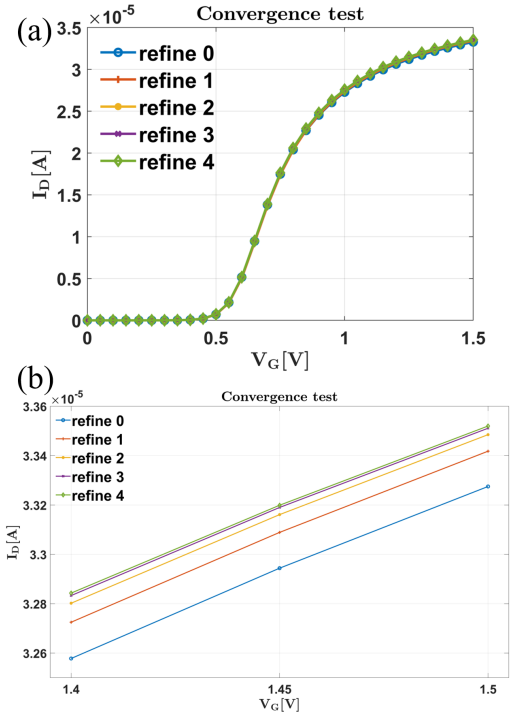

Fig. 3. (a) Transfer characteristics (I_D-V_G) computed using the EAFE scheme under mesh refinement levels from 0 to 4. The solution at refine level 4 (21,872,640 tetrahedra) is taken as the reference. (b) Local magnification at $V_G = 1.4 \sim 1.5$ V, showing convergence of I_D with refinement.

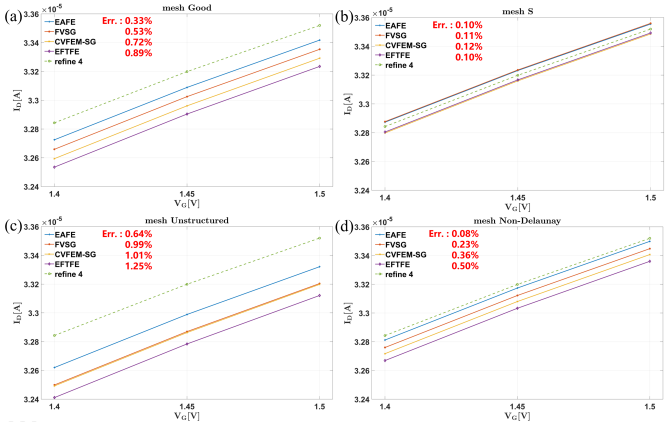

Fig. 4. Transfer characteristics (I_D-V_G) obtained using four discretization schemes (EAFE, FVSG, CVFEM-SG, EFTFE) on four mesh types. The EAFE method consistently delivers the highest accuracy and stability across all meshes. Simulations on mesh S exhibit the least sensitivity to discretization artifacts and geometric irregularities.

Fig. 3(a) presents the I_D-V_G characteristics obtained with the EAFE scheme, as the mesh is refined from level 0 (5,340 tetrahedra) to level 4 (21,872,640 tetrahedra) under a drain bias $V_D = 0.05\,\mathrm{V}$. The result from refinement level 4 is used as a reference solution. As seen in the magnified view in Fig. 3(b), the drain current converges with mesh refinement, demonstrating the accuracy and mesh independence of the numerical solution. Fig. 4 compares the I_D-V_G curves obtained from all four discretization methods across the four mesh types. Among them, EAFE consistently produces the lowest relative error and demonstrates strong robustness across different mesh qualities. Moreover, simulations based on the commercial mesh (mesh S) exhibit the least sensitivity to discretization and geometric irregularities.

To further analyze the stability of the discretization schemes and the efficiency of the associated linear solvers, Fig. 5 displays the maximum gate and drain bias values at which each method successfully converges. Fig. 6 presents the average number of FGMRES iterations per nonlinear step as the drain bias increases, with $V_G = 1.0\,\mathrm{V}$. The EAFE method not only achieves convergence at higher bias voltages across all mesh types, but also maintains stable iteration counts as the bias increases. To gain deeper insight into the impact of discretization, we analyze the spatial distribution of the quasi-Fermi potential. A 2D cross-sectional slice, perpendicular to the channel and located at the device midpoint, is extracted at $V_G = 1.5\,\mathrm{V}$ and $V_D = 0.05\,\mathrm{V}$. Fig. 7 - Fig. 10 show the corresponding quasi-Fermi potential distributions computed using the four methods across the four mesh types. On mesh Good, the potential remains nearly uniform across the slice, reflecting high numerical fidelity. On the other meshes, however, significant deviations appear, especially for CVFEM-SG and EFTFE. In contrast, the EAFE and FVSG methods yield smoother and more physically consistent distributions.

		mesh Good	mesh S	mesh Unstructured	mesh Non-Delaunay
$I_D - V_G$ $V_D = 0.7V$ increase V_G	EAFE	23.75V	31.55V	24V	30.8V
	FVSG	24.75V	31.55V	25.25V	35V
	Exp(Gummel)	0.25V	0.25V	0.25V	0.25V
	CVFEM-SG	24.3V	×($V_b = 0.55V$)	×($V_b = 0.25V$)	30.05V
$I_D - V_D$ $V_G = 1.0V$ increase V_D	EAFE	86.8V	100V	100V	100V
	FVSG	86.8V	100V	100V	55.7V
	Exp(Gummel)	0.55V	0.55V	0.55V	0.55V
	CVFEM-SG	14.95V	1.9V	0.75V	4.05V

Fig. 5. Maximum gate and drain bias values for which convergence was achieved under each discretization scheme and mesh type. The results reflect the robustness and stability of each method, with EAFE demonstrating the most reliable convergence behavior.

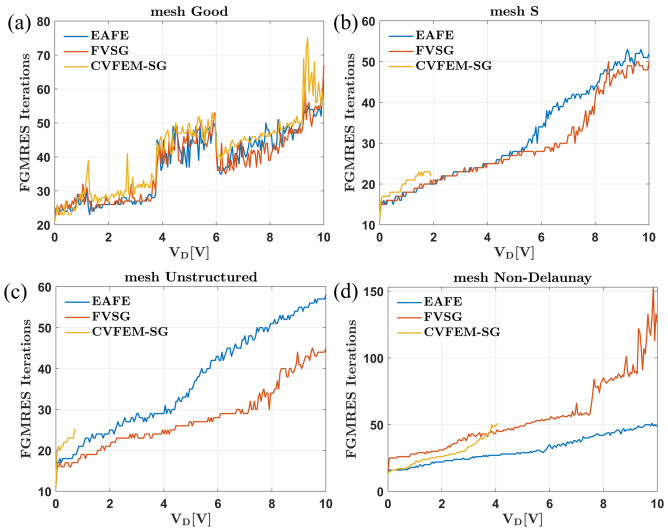

Fig. 6. Average number of FGMRES iterations per nonlinear step under increasing drain bias at $V_G = 1.0\,\mathrm{V}$. EAFE maintains a consistently low iteration count across all mesh configurations.

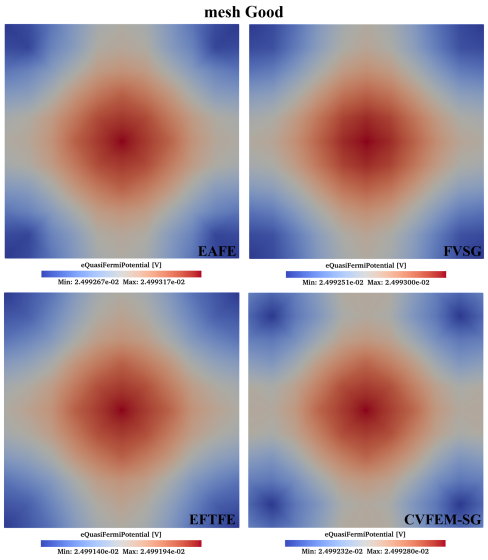

Fig. 7. Electron quasi-Fermi potential along a central cross-sectional slice of the GAA channel at $V_G = 1.5\,\mathrm{V}$, $V_D = 0.05\,\mathrm{V}$, using different discretization schemes on Mesh Good.

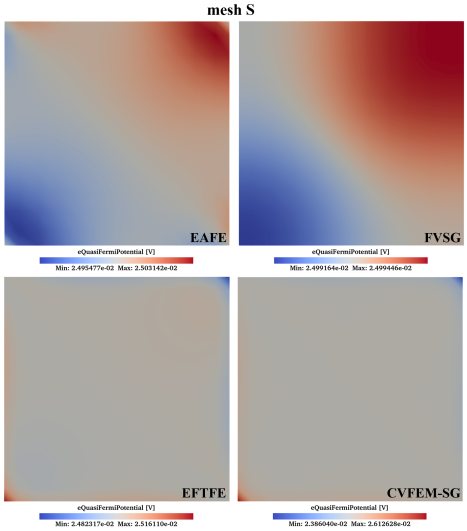

Fig. 8. Electron quasi-Fermi potential on the same slice and bias condition as in Fig. 7, simulated on mesh S.

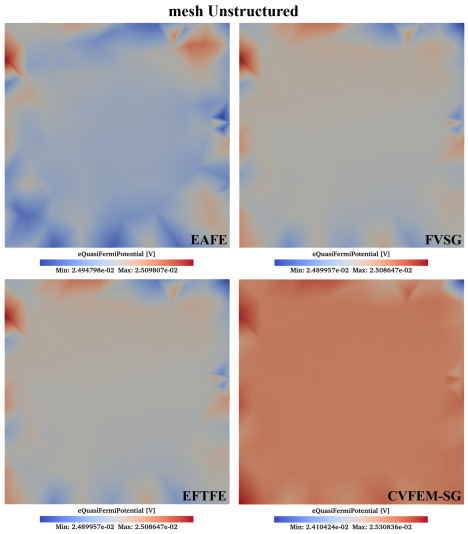

Fig. 9. Electron quasi-Fermi potential on the same slice and bias condition as in Fig. 7, simulated on mesh Unstructured.

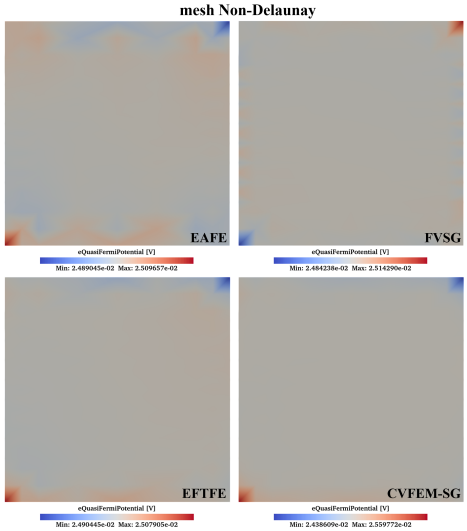

Fig. 10. Electron quasi-Fermi potential on the same slice and bias condition as in Fig. 7, simulated on mesh Non-Delaunay.

IV. Conclusion

We have systematically compared four representative discretization methods for the quasi-Fermi-level-based QDD model on various tetrahedral mesh types, including structured, unstructured, and non-Delaunay grids. Among them, EAFE shows the best overall performance in terms of accuracy, convergence stability, and robustness to mesh irregularity. These results highlight EAFE's suitability for advanced device simulations where process-induced geometric variations are significant. The findings also suggest that careful selection of discretization schemes is essential for ensuring reliable simulation of quantum-confined devices.

Acknowledgment

This work was supported by the Strategic Priority Research Program of Chinese Academy of Sciences (No. XDB0640303), the National Natural Science Foundation of China (No. 12401550), and the Process Physical Models and Simulation Tools (No. QYJS-2023-3002-B).

References

[1] K. Rupp, M. Bina, Y. Wimmer, A. Jungel, and T. Crasser, "Cell-centered finite volume schemes for semiconductor device simulation," in *2014 International Conference on Simulation of Semiconductor Processes and Devices (SISPAD)*, 2014, pp. 365–368.

[2] D. J. Cummings, M. E. Law, S. Cea, and T. Linton, "Comparison of discretization methods for device simulation," in *2009 International Conference on Simulation of Semiconductor Processes and Devices (SISPAD)*, 2009, pp. 1–4.

[3] S. Pérez-Escudero, D. Codony, I. Arias, and S. Fernández-Méndez, "A comparison of formulations and non-linear solvers for computational modelling of semiconductor devices," *Computational Mechanics*, 2024.

[4] J. Xu and L. Zikatanov, "A monotone finite element scheme for convection-diffusion equations," *Mathematics of Computation*, vol. 68, no. 228, pp. 1429–1446, 1999.

[5] P. Bochev, K. Peterson, and X. Gao, "A new control volume finite element method for the stable and accurate solution of the drift–diffusion equations on general unstructured grids," *Computer Methods in Applied Mechanics and Engineering*, vol. 254, pp. 126–145, 2013.

[6] L. Angermann and S. Wang, "Three-dimensional exponentially fitted conforming tetrahedral finite elements for the semiconductor continuity equations," *Applied Numerical Mathematics*, vol. 46, no. 1, pp. 19–43, 2003.

[7] Z. Stanojević, J. M. González-Medina, F. Schanovsky, and M. Karner, "Quasi-Fermi-based charge transport scheme for device simulation in cryogenic, wide bandgap, and high-voltage applications," *IEEE Transactions on Electron Devices*, vol. 70, no. 2, pp. 708–713, 2023.

[8] P. Mu, T. Cui, L. Xu, K. Luo, Z. Li, and Z. Wu, "A finite element framework for solving the density-gradient model," in *2024 International Conference on Simulation of Semiconductor Processes and Devices (SISPAD)*, 2024, pp. 1–4.

[9] H. Si, "Tetgen, a Delaunay-based quality tetrahedral mesh generator," *ACM Transactions on Mathematical Software*, vol. 41, no. 2, 2015.